


RESEARCH ARTICLE | APRIL 14 2017

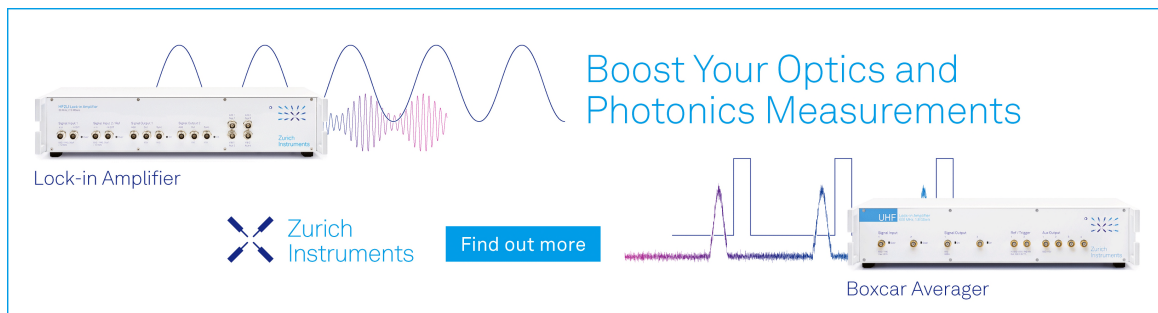
Chemical pressure effect in Sm and La substituted ferroelectric BiFeO₃ thin films: Insights from infrared spectroscopy

F. Burkert; M. Janowski; X. Zhang; I. Takeuchi; C. A. Kuntscher

 Check for updates


J. Appl. Phys. 121, 144103 (2017)

<https://doi.org/10.1063/1.4980105>



Boost Your Optics and Photonics Measurements

Lock-in Amplifier

 Zurich Instruments

[Find out more](#)

Boxcar Averager

Chemical pressure effect in Sm and La substituted ferroelectric BiFeO₃ thin films: Insights from infrared spectroscopy

F. Burkert,¹ M. Janowski,¹ X. Zhang,² I. Takeuchi,³ and C. A. Kuntscher^{1,a)}

¹Experimentalphysik 2, Universität Augsburg, D-86159 Augsburg, Germany

²Department of Physics, University of Maryland, College Park, Maryland 20742, USA

³Department of Materials Science and Engineering, University of Maryland, College Park, Maryland 20742, USA

(Received 23 January 2017; accepted 31 March 2017; published online 14 April 2017)

We investigate the effects of Sm and La substitution in ferroelectric BiFeO₃ thin films on the lattice dynamics by infrared reflection measurements at room temperature. The frequencies of the infrared-active phonon modes are studied as a function of Sm and La content in Bi_{1-x}(Sm,La)_xFeO₃ composition spread films in the range from $x = 0$ up to $x = 0.25$, grown on SrTiO₃ substrates by pulsed laser deposition. Substitution of the Bi³⁺ ions with small Sm³⁺ ions leads to the appearance of a new phase above $x \approx 0.09$ coexisting with the ferroelectric BiFeO₃ phase up to $x \approx 0.19$. In contrast, for the substitution of Bi³⁺ ions with La³⁺ ions of similar size a continuous transition from the original BiFeO₃ phase to a new phase takes place. In both cases, we assign the new phase to the paraelectric, orthorhombic phase. These findings are discussed in terms of the morphotropic phase boundary in Sm-doped BiFeO₃ around $x = 0.14$ with a phase coexistence, which was suggested as the origin for enhanced piezoelectric properties. *Published by AIP Publishing.*

[<http://dx.doi.org/10.1063/1.4980105>]

I. INTRODUCTION

The perovskite BiFeO₃ is a well-known magnetoelectric multiferroic with a rhombohedral structure with space group *R3c* at room temperature.^{1,2} BiFeO₃ shows both ferroelectricity,³ caused by the Bi 6s² lone pair electrons,^{4,5} and antiferromagnetism.⁶ The material has attracted a lot of attention due to its high antiferromagnetic ($T_N \approx 645$ K) and ferroelectric ($T_C \approx 1114$ K) transition temperatures,^{1,7} which make BiFeO₃ one of the very few examples for a single-phase multiferroic material above room temperature.⁸ BiFeO₃ furthermore raised tremendous interest as an interesting lead-free piezoelectric,^{9–11} however, with piezoelectric coefficients much smaller than Pb-based piezoelectrics. It is known that the material properties of piezoelectric oxides can be improved by doping. Some phase boundaries induced by composition changes, so-called morphotropic phase boundaries (MPBs), for example show enhanced piezoelectric and dielectric responses,¹² as demonstrated in ferroelectric Pb(Zr,Ti)O₃. Here, the competition between two structural phases at the MPB leads to enhanced piezoelectric and dielectric properties.^{13,14}

Chemical substitution has therefore been applied also to BiFeO₃ in order to improve its electromechanical properties, namely by replacing Bi³⁺ by rare-earth ions. Indeed, an enhanced piezoelectric response was observed for substitution by small rare-earth ions (Sm³⁺, Gd³⁺, and Dy³⁺),¹⁵ which induce a large chemical pressure in the system. For example, in case of Sm-doped Bi_{1-x}Sm_xFeO₃ a structural phase transition is induced with increasing doping level x from the ferroelectric rhombohedral phase to a paraelectric orthorhombic phase, leading to an enhancement of the

piezoelectric coefficient with a maximum at $x = 0.14$.^{11,15–17} A nano-scale phase coexistence of the rhombohedral ferroelectric phase, an antipolar PbZrO₃-like phase, and an orthorhombic paraelectric phase at the structural phase boundary was suggested as the driving mechanism for the enhancement.^{17–19} A nanodomain structure at the MPB was also found in the ferroelectric solid solution PbZr_xTi_{1-x}O₃.^{20–22}

In contrast, substitution of Bi³⁺ by La³⁺ with a comparable ionic size has a negligible weak chemical pressure effect. In La-doped BiFeO₃, no enhancement of the piezoelectric properties was found, despite the fact that a structural phase transition from the rhombohedral ferroelectric phase to an orthorhombic paraelectric phase is also induced by La doping.¹⁶ But the transition region was found to be broader compared to Sm-doped BiFeO₃ and no nanoscale phase coexistence was observed in case of La doping.^{16,19,23–27} A recent Raman study on Bi_{1-x}La_xFeO₃ suggested a structural phase transition from ferroelectric rhombohedral to an antiferroelectric PbZrO₃-like structure with signs of phase mixture, and finally to the LaFeO₃-type orthorhombic structure with further increasing La content.²⁷ However, these findings are inconsistent with the earlier results on the structural evolution in Bi_{1-x}La_xFeO₃ with increasing doping level x ,¹⁶ which might be due to the different type of studied sample (namely bulk sample in the former case, while thin film in the latter case). Furthermore, a corresponding detailed spectroscopic investigation of the structural phase transition in Sm-doped BiFeO₃ as a function of doping concentration is lacking so far.

In this work, we present a detailed investigation of the lattice dynamical properties in Sm- and La-substituted BiFeO₃ thin films during the doping-induced structural phase transition by means of infrared spectroscopy. The analysis of

^{a)}Electronic mail: christine.kuntscher@physik.uni-augsburg.de

the phonon mode spectrum as a function of Sm- and La-doping gives an insight into the structural changes in the material when driven towards the structural phase boundary in both cases, and allows a conclusion about the chemical pressure effects in BiFeO₃ caused by rare-earth substitution.

II. METHODS

The investigated BiFeO₃ composition spread films with a thickness of about 100 nm on ≈ 1 mm thick (100) SrTiO₃ (STO) substrates were fabricated by combinatorial pulsed laser deposition under epitaxial synthesis conditions with an automated moving shutter.^{11,16} The films were doped with Sm and La, respectively. The dopant concentration increased from 0% to 25% along both samples. Twelve measurement positions were defined on each sample (see Fig. 1).

The reflectivity measurements were performed with a Bruker IRScopeII infrared microscope, coupled to a Bruker IFS66v/S Fourier transform infrared spectrometer in the frequency range 100–700 cm⁻¹ with a resolution of 1 cm⁻¹. A bolometer attached to the microscope was used as a detector. As reference, we used the intensity reflected by an aluminum coated mirror. The samples were placed and aligned on a motorized stage of the infrared microscope, so that the measurement positions could be approached precisely and reproducibly. The size of the probing spot amounts to 250 μ m.

III. RESULTS AND DISCUSSION

The reflectance spectra in the frequency range between 100 cm⁻¹ and 700 cm⁻¹ were measured for both Sm- and La-doped BiFeO₃ composition spread films at the given positions. We observe a noticeable change of the reflectivity between the undoped ($x = 0$) and maximum doped ($x = 0.25$) positions on each film (see Fig. 2), especially in the range between 200 cm⁻¹ and 475 cm⁻¹. The reflectivity spectra are similar for both films at the undoped positions and are

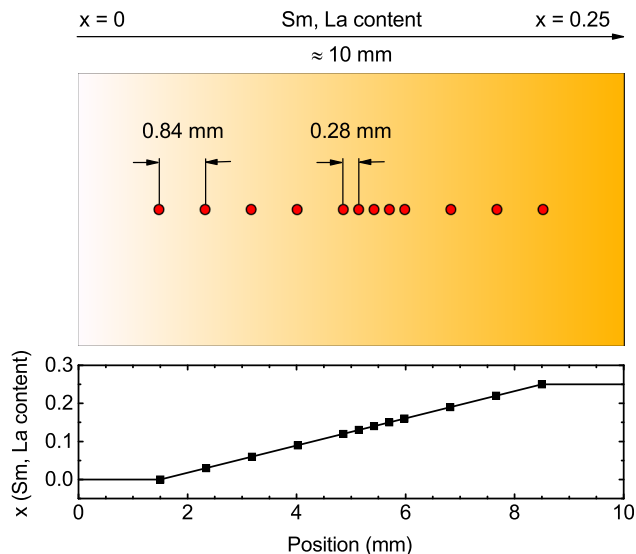


FIG. 1. Sketch of the sample geometry. The red circles indicate the measuring spots (marked spot size not in scale). Note that the spots lie closer to each other around the expected position of the MPB in Sm-doped BiFeO₃. The graph below shows the corresponding dopant concentration gradient.

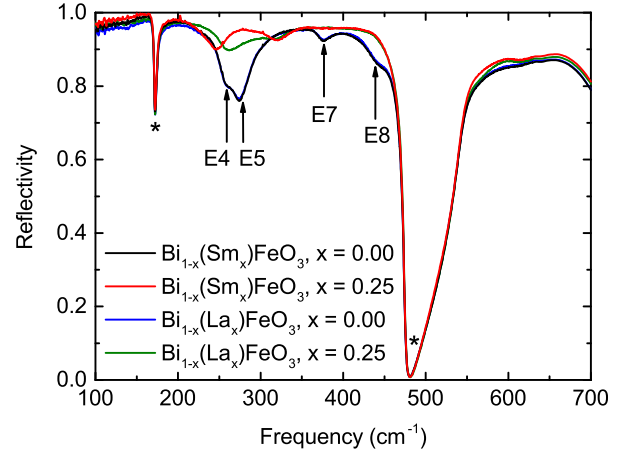


FIG. 2. Reflectivity of undoped ($x=0$) and maximum doped ($x=0.25$) BiFeO₃ films. The strongest modes of BiFeO₃ are labeled according to the literature.²⁸ The strong features around 172 cm⁻¹ and 481 cm⁻¹ marked with asterisks are due to excitations in the STO substrate.^{30–32}

consistent with earlier reports on pure BiFeO₃.^{28,29} However, the phonon mode spectra of Sm- and La-doped BiFeO₃ clearly differ at the maximum doped positions for frequencies between 200 cm⁻¹ and 350 cm⁻¹ (see Fig. 2). Above 350 cm⁻¹, the changes in reflectivity seem to be independent of the kind of dopant. The detailed enlargement in Fig. 3 shows the continuous change in the reflectivity spectrum with increasing dopant content for both films.

The reflectivity spectra were fitted using a two-layer model to represent the sample geometry. The STO substrate layer contribution was simulated by a four-parameter model according to literature data.^{31,33} For fitting the BiFeO₃

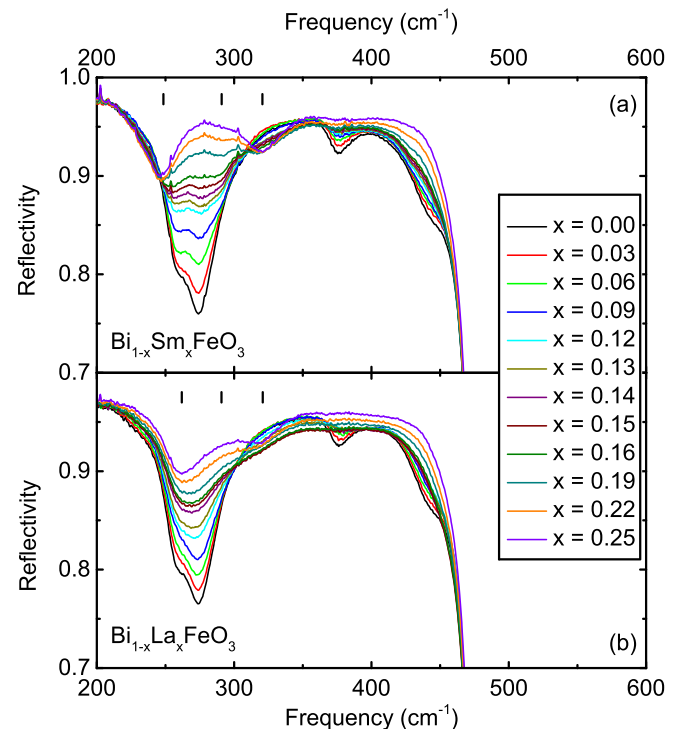


FIG. 3. Evolution of the reflectivity with increasing dopant content for (a) Bi_{1-x}Sm_xFeO₃ and (b) Bi_{1-x}La_xFeO₃. The ticks mark the three strongest modes for maximum doping $x = 0.25$ in both cases.

sample layer, we used a Lorentz model as described in Equations (1)–(3). The data given by Lobo *et al.*, who report nine optical phonon modes in the *ab* plane, were used as a guideline for the fitting parameters $\Delta\epsilon_j$, ω_j , and γ_j ²⁸

$$\hat{\epsilon}(\omega) = \epsilon_\infty + \sum_{j=1}^N \epsilon_{1,j} + i\epsilon_{2,j}, \quad (1)$$

$$\epsilon_{1,j}(\omega) = \frac{\Delta\epsilon_j \omega_j^2 (\omega_j^2 - \omega^2)}{(\omega_j^2 - \omega^2)^2 + \gamma_j^2 \omega^2}, \quad (2)$$

$$\epsilon_{2,j}(\omega) = \frac{\Delta\epsilon_j \omega_j^2 (\gamma_j \omega)}{(\omega_j^2 - \omega^2)^2 + \gamma_j^2 \omega^2}. \quad (3)$$

The phonon mode frequencies extracted from the fittings are listed in Table I for the undoped and maximum doped positions for both Sm- and La-doped BiFeO₃ films. The labeling of phonon modes was done according to Ref. 28. According to group theory, nine *E* modes are expected for pure BiFeO₃.²⁸

The phonon modes belong to three groups located in the frequency ranges 100–200 cm⁻¹, 200–400 cm⁻¹, and 400–850 cm⁻¹. Based on a comparison with other perovskite-type materials,^{34,35} they can be assigned to external vibrational modes of the FeO₆ octahedra against the Bi³⁺-ions and the FeO₆ octahedral bending and stretching modes, respectively.

In our reflectivity spectra, mode E2 and mode E9 are covered by noise or SrTiO₃ excitations, respectively, nevertheless we keep them for improving the fitting. Furthermore, modes E3 and E6 have a very low oscillator strength. There is a discrepancy of up to 5 cm⁻¹ in the mode frequencies in our films compared to the single-crystal results. The larger discrepancy for the E3 mode frequency is attributed to the rather large error bar, since this phonon mode appears in our reflectivity spectra as a very weak feature. We will concentrate in our discussion of the doping-induced changes on the evolution of the strong phonon modes in the obtained reflectivity spectra, namely the modes E4, E5, E7, and E8.

TABLE I. Oscillator frequencies from the fitting (in cm⁻¹).

	Bi _{1-x} Sm _x FeO ₃		Bi _{1-x} La _x FeO ₃	
	x = 0.00	x = 0.25	x = 0.00	x = 0.25
Mode E2 ^a	126.0	126.0	126.0	126.0
Mode E3	229.5	229.5	229.5	229.5 ^b
Mode E*	...	248.2
Mode E4	259.0	...	259.0	...
Mode E5	278.9	...	278.9	262.0
Mode E**	...	290.9	...	290.9
Mode E***	...	320.5	...	320.5
Mode E6 ^b	340.0	340.0	340.0	340.0
Mode E7	376.5	376.5 ^b	376.5	376.5 ^b
Mode E8	437.9	...	439.7	...
Mode E9 ^c	521.0	521.0	521.0	521.0

^aCovered by noise.

^bVery weak.

^cCovered by SrTiO₃ feature.

With increasing Sm-doping, the main changes in the phonon mode spectrum are the following [Fig. 3(a)]: First, three new phonon modes appear with frequencies at around 248 cm⁻¹, 291 cm⁻¹, and 321 cm⁻¹, which are labelled E*, E**, and E***. All three modes start to appear at $x \approx 0.09$, continuously gain oscillator strength with increasing doping, and reach maximum oscillator strength for $x \approx 0.19$. Simultaneously, the modes E4, E5, and E8 of the rhombohedral ferroelectric phase start to lose intensity from $x \approx 0.09$ and have disappeared above $x \approx 0.19$. Hence, according to the phonon spectrum of (Bi,Sm)FeO₃ there is a phase mixture of the rhombohedral ferroelectric phase and a new phase in the Sm doping range $0.09 \leq x \leq 0.19$. The evolution of the relative oscillator strength ($\Delta\epsilon/\epsilon_{max}$) with doping concentration is illustrated in Fig. 4(a) for selected modes. The transition region with a phase mixture in case of Sm doping has a width of $\Delta x = 0.10$ and a center at $x = 0.14$, which is in very good agreement with literature data about the critical stoichiometry that leads to the rhombohedral-orthorhombic phase transition.^{11,12,16,26}

The changes in the La-doped BiFeO₃ film are markedly different, as illustrated by the evolution of the relative oscillator strength $\Delta\epsilon/\epsilon_{max}$ with doping concentration [see Fig. 4(b)]. The new mode E* is not observed for La doping. The new modes E** and E*** appear at higher dopant concentrations, namely E** at $x = 0.14$ and E*** at $x = 0.13$. The oscillator strength of mode E4 starts to decrease noticeably between $x = 0.13$ and $x = 0.14$, accompanied by a continuous frequency shift of mode E5 starting at $x = 0.12$ to lower frequencies. Mode E4 finally vanishes above $x = 0.22$. As the frequency shift of mode E5 is presumably not yet finished at

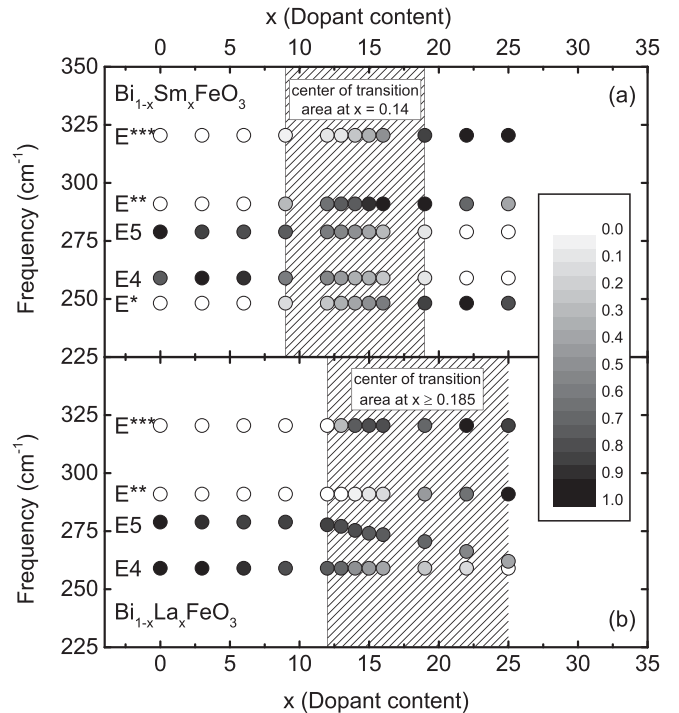


FIG. 4. Frequency of selected modes for (a) Bi_{1-x}Sm_xFeO₃ and (b) Bi_{1-x}La_xFeO₃ as a function of dopant content *x*. The relative oscillator strength $\Delta\epsilon/\epsilon_{max}$ is given as a gray scale of the circle filling. The hatched areas indicate the phase transition regions.

the last measurement position at $x = 0.25$, the width of the transition region can only be given as $\Delta x \geq 0.13$. The center of the broad transition region is located at $x \geq 0.185$. Literature data about the stoichiometry at the phase transition vary. Although some publications report the phase transition to occur at or even slightly below $x = 0.20$,^{25–27} other reports locate the phase transition at $x = 0.30$.^{12,16,24} This discrepancy may be explained by the broad transition range in $(\text{Bi,L a})\text{FeO}_3$.

In both doping cases, the phonon mode spectrum in the transition region does not clearly show the fingerprints of the predicted PbZrO_3 -type minority phase. The phonon mode spectrum of PbZrO_3 was characterized in Ref. 36 by infrared spectroscopy. Single crystalline PbZrO_3 exhibits eight transverse optical phonon modes, which should be observable in the room-temperature reflectivity spectrum. Since we observe only three strong modes in the doping-induced new phase, the occurrence of a PbZrO_3 -type phase cannot be confirmed based on our data. However, we cannot exclude the occurrence of this phase either, since part of the measured frequency range is masked by the strong STO substrate features.

The phases in $\text{Bi}_{1-x}\text{Sm}_x\text{FeO}_3$ and $\text{Bi}_{1-x}\text{La}_x\text{FeO}_3$ for the maximum doping level $x = 0.25$ are very similar regarding their phonon mode spectrum (see Fig. 2): In both cases, the spectrum consists of three strong modes. Two of these modes have the same frequencies (mode E^{**} at 291 cm^{-1} and mode E^{***} at 321 cm^{-1}). For $\text{Bi}_{0.75}\text{Sm}_{0.25}\text{FeO}_3$, the third mode (mode E^* at 248 cm^{-1}) is shifted to lower frequency compared to $\text{Bi}_{0.75}\text{La}_{0.25}\text{FeO}_3$ (mode $E5$ at 262 cm^{-1}). This suggests that in both cases the paraelectric orthorhombic phase (space group $Pnma$) has been reached for the doping concentration $x = 0.25$, consistent with results from x-ray diffraction.¹⁶ The difference in the frequency position of one mode could be attributed to the different sizes of Sm^{3+} and La^{3+} ions. Based on our results, we could conclude that the phase reached for the maximum doping level is similar in both Sm and La doping cases. For SmFeO_3 , no reports on the phonon mode spectrum exist until now. Therefore, we will compare the obtained phonon mode spectrum of $\text{Bi}_{0.75}\text{La}_{0.25}\text{FeO}_3$ with that of LaFeO_3 reported in the literature.³⁷ Since the lattice parameter still changes for doping levels above $x = 0.25$, as demonstrated for the out-of-plane lattice parameter,¹⁶ this comparison can only be carried out on a qualitative level. Monocrystalline LaFeO_3 (orthorhombic phase with space group $Pnma$) shows six transverse optical phonon modes with frequencies 164, 256, 278, 316, 399, and 534 cm^{-1} . For $\text{Bi}_{0.75}\text{La}_{0.25}\text{FeO}_3$, we measured three strong phonon modes at 262, 291, and 321 cm^{-1} , which are close in frequency to the modes reported for LaFeO_3 . The missing modes at 164, 399, and 534 cm^{-1} might be covered by the pronounced STO substrate features or too weak.

Importantly, the evolution of the structure from rhombohedral, ferroelectric BiFeO_3 phase to the orthorhombic, paraelectric phase at high doping concentration is markedly different for Sm and La substitution. This dopant-dependent evolution of the phonon mode spectrum during the structural phase transition in BiFeO_3 can be explained in terms of the different ionic sizes of the substitution elements. For a

coordination number of twelve, the ionic radius of La^{3+} (1.36 \AA) is similar to the one of Bi^{3+} (1.36 \AA), while the Sm^{3+} ion is significantly smaller (radius 1.28 \AA).¹⁹ Accordingly, the La^{3+} substitution constitutes a negligible weak chemical pressure case. Hence, La^{3+} gradually substitutes the similar-sized Bi^{3+} ions within the rhombohedral, ferroelectric phase, leading to a single $\text{Bi}_{1-x}\text{La}_x\text{FeO}_3$ phase and a continuous phase transition from the rhombohedral BiFeO_3 phase towards the orthorhombic, paraelectric LaFeO_3 phase with space group $Pnma$. The structural changes due to La substitution are caused by the dilution of the stereochemically active Bi $6s^2$ lone-pair electrons, which are considered responsible for the ferroelectric displacements in BiFeO_3 .^{4,5} The gradual substitution of Bi by La also causes the continuous frequency shift of the mode $E5$, which is an FeO_6 octahedral bending mode.^{34,35} Such a scenario of the structural evolution with increasing La-doping would be consistent with the continuous evolution of the out-of-plane lattice parameter for La-doped BiFeO_3 as reported in Ref. 16.

However, the Sm^{3+} ions are too small to fit into the original Bi^{3+} phase and therefore constitute a strong chemical pressure case. In contrast to La doping, the Sm^{3+} ions build up a new paraelectric, orthorhombic phase starting from $x = 0.09$, which coexists with the original Bi^{3+} phase. With increasing Sm content, the fraction of the orthorhombic, paraelectric phase increases at the expense of the ferroelectric BiFeO_3 phase fraction, which has disappeared completely for $x = 0.19$. Accordingly, the oscillator strength of the phonon modes of the BFO phase decreases in the transition region $0.09 \leq x \leq 0.19$, while the oscillator strength of the new modes increases. As expected under this condition, the phonon mode frequencies are stable. The proposed scenario is consistent with the observed phase coexistence at the structural phase boundary, which was suggested as the driving mechanism for the enhancement of the piezoelectric coefficient expected at a MPB.^{16,19} Please note that we do not observe the signatures of the antipolar PbZrO_3 -like phase in the phonon mode spectra of $\text{Bi}_{1-x}\text{Sm}_x\text{FeO}_3$. As this phase is a minority phase on a nanometer scale,¹⁶ the corresponding fingerprints in the phonon mode spectrum might be too weak to be observable as we average over a relatively large area of the film with a probing spot size of $250\text{ }\mu\text{m}$. Also, it needs to be mentioned that strong STO substrate features cover part of the measured frequency range, which could mask the fingerprints of the PbZrO_3 -like minority phase.

IV. CONCLUSION

We have studied the phonon mode spectrum of $\text{Bi}_{1-x}\text{Sm}_x\text{FeO}_3$ and $\text{Bi}_{1-x}\text{La}_x\text{FeO}_3$ composition spread films up to a doping level of $x = 0.25$ by reflectivity measurements at room temperature. With increasing dopant content, we observe significant changes like appearance, vanishing, and shifting of phonon modes during the phase transition from the ferroelectric rhombohedral phase to the paraelectric orthorhombic phase, which significantly depends on the dopant element. This behaviour can be explained by the different sizes of the dopant ions. In case of Sm-doping, which causes a strong chemical pressure, our findings are consistent with

the proposed phase coexistence of the rhombohedral, ferroelectric BiFeO₃ phase with the paraelectric, orthorhombic phase at the structural phase boundary, which was suggested to cause an enhancement of the piezoelectric coefficient typically observed in piezoelectrics at the morphotropic phase boundary. The phonon mode spectrum for Bi_{1-x}La_xFeO₃ is interpreted in terms of a continuous phase transition from the rhombohedral BiFeO₃ phase towards the orthorhombic, paraelectric LaFeO₃ phase. Neither for Sm doping nor for La doping we find the fingerprints of the predicted PbZrO₃-like minority phase in the reflectivity spectra. They might be too weak or masked by the strong features related to the STO substrate.

ACKNOWLEDGMENTS

This work was financially supported by the Deutsche Forschungsgemeinschaft (DFG) through Grant No. KU 1432/9-1.

- ¹J. M. Moreau, C. Michel, R. Gerson, and W. J. James, *J. Phys. Chem. Solids* **32**, 1315 (1971).
- ²F. Kubel and H. Schmid, *Acta Cryst. Sec. B* **46**, 698 (1990).
- ³J. R. Teague, R. Gerson, and W. J. James, *Solid State Commun.* **8**, 1073 (1970).
- ⁴P. Ravindran, R. Vidya, A. Kjekshus, H. Fjellvåg, and O. Eriksson, *Phys. Rev. B* **74**, 224412 (2006).
- ⁵G. Catalan and J. F. Scott, *Adv. Mater.* **21**, 2463 (2009).
- ⁶I. Sosnowska, T. Peterlin-Neumaier, and E. Steichele, *J. Phys. C: Solid State Phys.* **15**, 4835 (1982).
- ⁷V. G. Bhide and M. S. Multani, *Solid State Commun.* **3**, 271 (1965).
- ⁸B. Ramachandran, A. Dixit, R. Naik, G. Lawes, and M. S. R. Rao, *Phys. Rev. B* **82**, 012102 (2010).
- ⁹J. Wang, *Science* **299**, 1719 (2003).
- ¹⁰D. Lebeugle, D. Colson, A. Forget, M. Viret, P. Bonville, J. F. Marucco, and S. Fusil, *Phys. Rev. B* **76**, 024116 (2007).
- ¹¹S. Fujino, M. Murakami, V. Anbusathaiah, S.-H. Lim, V. Nagarajan, C. J. Fennie, M. Wuttig, L. Salamanca-Riba, and I. Takeuchi, *Appl. Phys. Lett.* **92**, 202904 (2008).
- ¹²J.-H. Lee, M.-A. Oak, H. J. Choi, J. Y. Son, and H. M. Jang, *J. Mater. Chem.* **22**, 1667 (2012).
- ¹³B. Noheda, J. A. Gonzhalo, L. E. Cross, R. Guo, S. E. Park, D. E. Cox, and G. Shirane, *Phys. Rev. B* **61**, 8687 (2000).
- ¹⁴B. Jaffe, W. R. Cook, and H. Jaffe, *Piezoelectric Ceramics* (Academic Press, London, New York, 1971).
- ¹⁵D. Kan and I. Takeuchi, *J. Appl. Phys.* **108**, 14104 (2010).
- ¹⁶D. Kan, C.-J. Cheng, V. Nagarajan, and I. Takeuchi, *J. Appl. Phys.* **110**, 14106 (2011).
- ¹⁷C.-J. Cheng, D. Kan, V. Anbusathaiah, I. Takeuchi, and V. Nagarajan, *Appl. Phys. Lett.* **97**, 212905 (2010).
- ¹⁸S. B. Emery, C.-J. Cheng, D. Kan, F. J. Rueckert, S. P. Alpay, V. Nagarajan, I. Takeuchi, and B. O. Wells, *Appl. Phys. Lett.* **97**, 152902 (2010).
- ¹⁹C.-H. Yang, D. Kan, I. Takeuchi, V. Nagarajan, and J. Seidel, *Phys. Chem. Chem. Phys.* **14**, 15953 (2012).
- ²⁰D. I. Woodward, J. Knudsen, and I. M. Reaney, *Phys. Rev. B* **72**, 104110 (2005).
- ²¹K. A. Schönau, L. A. Schmitt, M. Knapp, H. Fuess, R.-A. Eichel, H. Kungl, and M. J. Hoffmann, *Phys. Rev. B* **75**, 184117 (2007).
- ²²G. A. Rossetti and A. G. Khachatryan, *Appl. Phys. Lett.* **91**, 072909 (2007).
- ²³S.-T. Zhang, Y. Zhang, M.-H. Lu, C.-L. Du, Y.-F. Chen, Z.-G. Liu, Y.-Y. Zhu, N.-B. Ming, and X. Q. Pan, *Appl. Phys. Lett.* **88**, 162901 (2006).
- ²⁴S.-T. Zhang, L.-H. Pang, Y. Zhang, M.-H. Lu, and Y.-F. Chen, *J. Appl. Phys.* **100**, 114108 (2006).
- ²⁵I. O. Troyanchuk, M. V. Bushinsky, D. V. Karpinsky, O. S. Mantytskaya, V. V. Fedotova, and O. I. Prochnenko, *Phys. Status Solidi B* **246**, 1901 (2009).
- ²⁶S. Karimi, I. M. Reaney, Y. Han, J. Pokorny, and I. Sterianou, *J. Mater. Sci.* **44**, 5102 (2009).
- ²⁷J. Bielecki, P. Svedlindh, D. T. Tibebe, S. Cai, S.-G. Eriksson, L. Börjesson, and C. S. Knee, *Phys. Rev. B* **86**, 184422 (2012).
- ²⁸R. Lobo, R. Moreira, D. Lebeugle, and D. Colson, *Phys. Rev. B* **76**, 172105 (2007).
- ²⁹S. Kamba, D. Nuzhnyy, M. Savinov, J. Šebek, J. Petzelt, J. Prokleška, R. Haumont, and J. Kreisel, *Phys. Rev. B* **75**, 024403 (2007).
- ³⁰J. Galzerani and R. Katiyar, *Solid State Commun.* **41**, 515 (1982).
- ³¹I. Fedorov, V. Železný, J. Petzelt, V. Trepakov, M. Jelínek, V. Trtík, M. Černanský, and V. Studnička, *Ferroelectrics* **208–209**, 413 (1998).
- ³²B. Almeida, A. Pietka, P. Caldelas, J. Mendes, and J. Ribeiro, *Thin Solid Films* **513**, 275 (2006).
- ³³K. Kamarás, K.-L. Barth, F. Keilmann, R. Henn, M. Reedyk, C. Thomsen, M. Cardona, J. Kircher, P. L. Richards, and J.-L. Stehlé, *J. Appl. Phys.* **78**, 1235 (1995).
- ³⁴J. T. Last, *Phys. Rev.* **105**, 1740 (1957).
- ³⁵K. Thirunavukkuarasu, F. Lichtenberg, and C. A. Kuntscher, *J. Phys.: Condens. Matter* **18**, 9173 (2006).
- ³⁶T. Ostapchuk, J. Petzelt, V. Zelenzny, S. Kamba, B. Malic, M. Kosec, L. Cakare, K. Roleder, and J. Dec, *Ferroelectrics* **239**, 109 (2000).
- ³⁷M. Daturi, G. Busca, and R. J. Willey, *Chem. Mater.* **7**, 2115 (1995).